Geophys. J. Int. (2003) **152,** 433–442

Determination of thermal conductivity and formation temperature from cooling history of friction-heated probes

Tien-Chang Lee,[1] A. D. Duchkov[2] and S. G. Morozov[2]

[1] *Department of Earth Sciences, University of California, Riverside,* CA 92521*, USA. E-mail: Tien.Lee@UCR.EDU*
[2] *Institute of Geophysics SB RAS, Prosp. Akad. Koptyuga* 3*, Novosibirsk,* 630090 *Russia*

Accepted 2002 August 12. Received 2002 July 8; in original form 2001 November 19

SUMMARY

The formation temperature below the sea or lake floor is frequently measured with a sensor probe that is inserted into the unconsolidated sediment, and the thermal conductivity of sediment is measured *in situ* with an independent heating experiment. Friction during the insertion raises the temperature of a probe. This paper presents the method and the test results of using the cooling history of friction-heated probes for the determination of equilibrium formation temperature and thermal conductivity. The inverse modelling (IM) for the desired parameters is formulated together with the finite-element simulation of the cooling history. The starting parameter values for IM are generated with a genetic algorithm (GA) that searches for them in the likely parameter ranges. The IM is constrained in an objective function by a commonly used asymptotic relation between the declining temperature and the inverse time. In addition to satisfying the root-mean-square misfit, the results are assessed by the equality between the model conductivity and the conductivity obtained through the asymptotic relation and by how well the models can predict the cooling behaviour at time beyond the record period for IM. The results of testing synthetic data with random noise up to ± 0.005 K and twenty 8–11 min long data sets from four sites in Lake Baikal indicate that the desired parameters can be determined from the first 2.5 min of the cooling records. By comparison with independent measurements or through repeated GA-IM, equilibrium temperatures can be consistently determined to within 0.002 K and thermal properties typically to ± 5 per cent. The method has also been successfully applied to seven sets of 5 min long data sets at one marine heat flow station.

Key words: formation temperature, heat flow, inverse modelling, Lake Baikal, thermal conductivity.

INTRODUCTION

A determination of terrestrial heat flow requires measurements of geothermal gradient and thermal conductivity of rocks or sediments. In the ocean floor or lake bottom, the determination is often accomplished with a device that bears sensor probes for measuring temperature and heater tubes as line sources for measuring conductivity. The temperature–conductivity (TC) device is driven into the unconsolidated sediments by freefall in the near-bottom water column or by high-speed impact. Frictional heating during insertion raises the temperature of a probe, which is usually but not always higher than the ambient formation temperature in the sediment where a probe finally rests. If the temperature of the probe is higher, it will decay eventually to the ambient formation temperature. This study explores the feasibility of using the cooling behaviour to determine the formation temperature and thermal conductivity.

Ideally, to measure the formation temperature, the sensor probes should stay stationary in the sediment until the friction-generated heat has dissipated sufficiently. In practice, rather than waiting for the complete heat dissipation at the rising cost of ship operational time and at the risk of disturbing the probes through unintended ship movement, a line-source-based asymptotic relation between temperature decay and inverse time has often been used to obtain the desired equilibrium temperature (Hyndman *et al.* 1979; Hutchison & Owen 1989; Jemsek & von Herzen 1989). This relation can be further utilized in the method presented here to constrain our inverse modelling for conductivity determination and to validate the estimate of formation temperature.

Conductivity measurement can be made either on sediment cores or *in situ*. Disturbance to the core, imperfect core recovery and mismatch between the core and sensor positions can affect the accuracy of heat flow determination. Being cumbersome and requiring extra time for coring preparation and core retrieval, coring cannot allow multiple penetrations for measurements of geothermal gradients at closely spaced stations. Based on a steady, continuous line-source method and made only after frictional heat has dissipated sufficiently or its residual heat can be confidently corrected, *in situ* measurements require extra battery power supply and

an additional 5–10 min to complete a heating experiment (Hyndman *et al.* 1979; Lister 1979; Jemsek & von Herzen 1989; Polyak *et al.* 1996).

Because the cooling history of a friction-heated probe reflects the heating event and physical properties, the idea of using a cooling curve for deducing the thermal properties has been contemplated since the first marine heat flow measurement (Bullard 1954). However, the idea could not be properly tested with the now antiquated analogue data. Using digital data, Lee & von Herzen (1994) tested whether the equilibrium temperature and the thermal conductivity are determinable from cooling curves at two marine heat-flow stations. Recently, we have acquired high-quality data from Lake Baikal. The much-improved quality of the data inspires us to further develop and test the methodology for using friction as a heat source for *in situ* determination of thermal conductivity and diffusivity.

The new development includes the following. (1) An empirical relation that links heat capacity with thermal conductivity as used by Lee & von Herzen (1994) is now abandoned. This paves the way at no extra cost for the determination of thermal diffusivity, which is needed for imposing heat flow as an energy constraint in transient heat-transfer modelling or for investigation of bottom water temperature variations, the effect of which is recorded in the sediments. (2) A genetic algorithm (GA) is employed to scan through reasonable ranges of parameter values so that potential pitfalls of a model converging towards a local minimum in the parameter space can be spotted. (3) A conductivity constraint based on the above-mentioned asymptotic relation for estimating equilibrium temperature is now formally incorporated into an objective function for inverting the parameters that define the cooling history of a probe. (4) The model parameters are assessed additionally to see whether a model can predict the cooling behaviour at a time beyond the record period used for modelling.

Our lake data were sampled at 2.5 s intervals (10 times as fine as the 26 s intervals used by Lee & von Herzen) and the recording was approximately twice the duration (approximately 5 min) of a typical measurement of geothermal gradient in the ocean floor. The high sampling frequency allows a better determination of the origin time when the sensor probe begins to act as an instantaneous line source, and justifies the usage of an ad hoc energy spreading factor that was proposed to facilitate curve fitting. In the absence of independent data for verification, the results of inverse modelling are often met with cautious acceptance even for models that satisfy certain model selection criteria. Provided with a long recording data set at a high sampling rate, we can use the first 2.5 min of the records for modelling and, on the basis of the resulted model parameters, curve-match the cooling behaviour for periods three times beyond the recording period (2.5 min) used for inverse modelling. Extrapolation fitting is hereby recognized as a viable means to confirm the modelling results if a method such as that presented herein is to be practised for measuring terrestrial heat flow through a lake or ocean floor.

Better depth and lateral resolution in heat flow measurements is desirable in areas of significant inhomogeneity in thermal properties and for investigation of advective heat flux (e.g. hydrothermal circulation) or of climate changes as imprinted in the sediments through bottom-water temperature variations (Davis *et al.* 1999; Barker & Lawver 2000). Many factors can affect the accuracy of heat flow determination and consequently the interpretation of data for geodynamic modelling (e.g. von Herzen *et al.* 2001). Those factors will not be dealt with in this paper. Interested readers can find the subject matter through recent correspondence by Geli *et al.* (2001), Davis *et al.* (2002) and Fisher *et al.* (2002). This paper illustrates a method that does not require an active heating experiment for conductivity measurements and that can extract the formation temperature from a short-duration recording. Such a method can save ship operation time, reduce the chance of disturbance to data recording caused by sensor movement, and allow for the design of finer spatial resolution in data acquisition. It is hoped that high spatial resolution in the determination of formation temperature and thermal properties can permit better evaluation of temperature–depth profiles that may have been affected by bottom-water temperature variation or advection of interstitial fluid.

In the following, we will briefly describe the cooling model, and then document the inverse modelling in detail. For bridging with previous work, we will also revisit seven test examples of Lee & von Herzen at one site at the Atlantic–continental margin.

COOLING MODEL

After frictional heating during the insertion, the probe and its surrounding sediment are assumed to cool conductively to the ambient equilibrium formation temperature θ_∞. With axial heat transfer neglected, heat conduction for an axisymmetric system in a homogeneous medium follows

$$\frac{\partial^2\theta}{\partial r^2} + \frac{1}{r}\frac{\partial\theta}{\partial r} = \frac{\rho c}{k}\frac{\partial\theta}{\partial t}, \tag{1}$$

where $\theta\,(r, t)$ is the temperature, r is the radial distance, t is the time, k is the thermal conductivity and ρc is the heat capacity at constant volume (see Appendix A for notation).

The thermal regime of interest consists of two media with distinctive thermal properties k and ρc, one representing the sensor probe (medium 1) and the other the sediments. The initial temperature is defined by

$$\begin{aligned}
&\theta_1(r, 0) = \theta_0, \quad r \le a;\\
&\theta_2(r, 0) = \theta_0 + \frac{r-a}{b-a}(\theta_b - \theta_0), \quad a \le r \le b;\\
&\theta_2(r, 0) = \theta_\infty, \quad b \le r \le c,
\end{aligned} \tag{2}$$

where a is the radius of the probe, b is the outer radius of a thin, disturbed sediment sheath around the probe, c is the proxy of infinite radial distance, θ_0 is the initial temperature in the probe, θ_∞ is the equilibrium formation temperature and θ_b is the initial temperature at $r = b$,

$$\theta_b = \theta_2(b, 0) = w\theta_0 + (1-w)\theta_\infty, \quad 0 < w < 1 \tag{3}$$

and w is a weighting factor between θ_0 and θ_∞, herein called the 'energy spreading factor'. The factor w represents the extent of spreading frictional heat energy into the sediments before the heat is assumed to be instantaneously released from a friction-heated probe. Being a parameter to be determined by inverse modelling, w was introduced by Lee & von Herzen (1994) for the convenience of compensating the mass disturbance and associated heat transfer during probe insertion.

The boundary conditions are

$$\left(\frac{\partial\theta_1}{\partial r}\right)_{r=0} = 0, \quad \theta_2(\infty, t) = \theta_2(c, t) = \theta_\infty, \quad 0 \le t < \infty. \tag{4}$$

The conditions at the interface $r = a$ are

$$\theta_1(a, t) = \theta_2(a, t), \left(k_1\frac{\partial\theta_1}{\partial r}\right)_{r=a} = \left(k_2\frac{\partial\theta_2}{\partial r}\right)_{r=a}. \tag{5}$$

The origin time of 'instantaneous heating' needs to be defined for modelling because the temperature at the instant when a probe stops descending in the sediment may not be recorded. A delay time t_D is introduced here as an additional parameter to represent the first recording time after the frictional heating. The effect of an uncertain t_D increases with increasing recording interval. Our cooling model is now fully described by the governing differential equation and the initial and the boundary conditions provided that eight model-defining parameters k_1, $(\rho c)_1$, k_2, $(\rho c)_2$, θ_0, θ_∞, w and t_D are given.

METHOD

Beginning with parameter searching using a genetic algorithm, the parameters are determined by inverse modelling (IM) through an iterative comparison of the simulated and observed cooling history. The simulation is made by a finite-element analysis (FE) for a given set of model parameters.

Finite-element analysis

Our simulation of the cooling history of a probe as forward modelling is based on 1-D axisymmetric finite-element analysis, for which the theoretical development is available in several textbooks. Our application follows those described in Lee & von Herzen (1994). A summary is presented below for documenting the method.

The region of interest between $r = 0$ and c is discretized into N_r ring (shell) elements with their ring thicknesses Δr increasing outward radially. The radius of the innermost ring (a cylinder) coincides with the probe radius a. The outermost ring radius c is approximately four times the diffusion distance $D = \sqrt{\kappa t_{end}}$, where κ is the thermal diffusivity and t_{end} is the final observation time. The number of rings N_r and ring thicknesses are estimated empirically. As an example for the test cases in Lake Baikal, $a = 3$, $b = 5$, $c =$ 63 mm (for $\kappa \approx 0.35 \times 10^{-6}$ m^2 s^{-1}, $t_{end} = 700$ s), $N_r = 24$ and $\Delta r = 2$–3 mm.

The temperature inside each element is linearly interpolated between the bounding nodal temperatures of the element. The initial temperature in excess above the equilibrium temperature is used to estimate the amount of energy released from a heated probe.

After minimizing the Galerkin weighted residual and using linear interpolation between two consecutive time steps, the governing eq. (1) and the initial and boundary conditions become a set of simultaneous equations for the nodal temperature vector θ^i at the end of time step i in terms of θ^{i-1} at the beginning,

$$\left(\mathbf{C} + \frac{2\Delta t}{3}\mathbf{K}\right)\theta^i = \left(\mathbf{C} - \frac{\Delta t}{3}\mathbf{K}\right)\theta^{i-1}, \quad i = 1, 2, 3, \ldots, \tag{6}$$

where the bold sans serif uppercase and bold lowercase letters denote matrices and column vectors, respectively, and Δt is the time span at step i. The global capacitance matrix $\mathbf{C}$ with a dimension of $(N_r + 1) \times (N_r + 1)$ is assembled from individual 2×2 elementary matrices

$$\mathbf{C}^e = \frac{\rho c\, \bar{r}\, \Delta r}{6}\begin{bmatrix} 2 & 1 \\ 1 & 2 \end{bmatrix}, \tag{7}$$

where $\bar{r}$ is the mean of the outer and inner radii for element e and Δr is its ring thickness. The global conductance matrix $\mathbf{K}$ is assembled similarly from individual elementary matrices

$$\mathbf{K}^e = \frac{k\,\bar{r}}{\Delta r}\begin{bmatrix} 1 & -1 \\ -1 & 1 \end{bmatrix}. \tag{8}$$

Within time step i, the $(N_r + 1) \times 1$ column vector θ^{i-1} represents the initial condition and θ^i is the final nodal temperature. This θ^i in time step i becomes θ^{i-1} in the next time step $i + 1$ for obtaining a set of new nodal temperatures θ^i. The process repeats for every time step. The step size Δt is either one-half or one-quarter of the sampling time interval for the FE modelling (the sampling interval for modelling can be less than the recording interval) except that Δt is made smaller in the first time step from time zero to time t_D.

The computed temperatures inside the probe at different times constitute the temperature vector $\mathbf{d}$ used in inverse modelling. For the purpose of modelling, the temperature of a probe is the weighted average of the temperatures at nodes 1 and 2.

Inverse modelling

For inverse modelling to determine the model-defining parameters, we apply an iterative Newton–Gauss method to a scalar objective function,

$$S = S^{\mathrm{I}} + S^{\mathrm{II}}, \tag{9}$$

where

$$S^{\mathrm{I}} = (\mathbf{d}^{\mathrm{obs}} - \mathbf{d})^{\mathrm{T}}\mathbf{C}_{\mathrm{d}}^{-1}(\mathbf{d}^{\mathrm{obs}} - \mathbf{d}) + (\mathbf{p}^{\mathrm{trial}} - \mathbf{p})^{\mathrm{T}}\mathbf{C}_{\mathrm{p}}^{-1}(\mathbf{p}^{\mathrm{trial}} - \mathbf{p}),$$
$$S^{\mathrm{II}} = (k_s/k_2 - 1)^2. \tag{10}$$

The first part S^{I} (Tarantola 1987; Lee & von Herzen 1994; Lee 1999) measures the misfits between the $N \times 1$ observed temperature vector $\mathbf{d}^{\mathrm{obs}}$ and the computed temperature vector $\mathbf{d}$ and the misfits between the $M \times 1$ trial parameter vector $\mathbf{p}^{\mathrm{trial}}$ and the iteratively determined parameter vector $\mathbf{p}$. $\mathbf{C}_{\mathrm{D}}$ and $\mathbf{C}_{\mathrm{p}}$ are the $N \times N$ covariance matrix of the data and the $M \times M$ covariance matrix of the parameters, respectively, with N being the number of the observed temperature data and M the number of parameters. The superscript T denotes the transpose of a matrix. The diagonal entries of $\mathbf{C}_{\mathrm{d}}$ and $\mathbf{C}_{\mathrm{p}}$ are the variances of the data and parameters, respectively. The differences between $\mathbf{d}^{\mathrm{obs}}$ and $\mathbf{d}$ and between $\mathbf{p}^{\mathrm{trial}}$ and $\mathbf{p}$ are assumed to have Gaussian distributions. The data are assumed to have no systematic error and the parameters are uncorrelated to one another such that the off-diagonal entries for the two covariance matrices are set to zero initially. As described in Tarantola (1987), the $\mathbf{p}^{\mathrm{trial}}$ represents prior knowledge but it is only a set of trial values as used here.

The second part S^{II} imposes the constraint of an asymptotic cooling behaviour. The temperature distribution arising from an instantaneous line sources in an infinite medium of conductivity k_s and thermal diffusivity κ is

$$\theta(r, t) = \theta_{\infty s} + \frac{Q}{4\pi k_s t}\exp(-r^2/4\kappa t), \tag{11}$$

where Q is the energy production per unit line length and $\theta_{\infty s}$ is the equilibrium temperature. At large times ($t \gg r^2/4\kappa$), the temperature behaves as

$$\theta(r, t) \approx \theta_{\infty s} + \frac{Q}{4\pi k_s t}. \tag{12}$$

A linear regression of θ versus $1/t$ yields an intercept of $\theta_{\infty s}$ and a slope of $\eta = Q/4\pi k_s$. This relation has been used frequently to estimate the equilibrium temperature from data recording that is short of reaching a thermal steady state (e.g. Hutchison & Owen 1989). The conductivity k_s can be estimated from the slope η if the frictional heat generation Q is determinable from curve fitting. Here we define a function

$$f^2 = \left(\frac{Q}{4\pi k_2 \eta} - 1\right)^2 = S^{\mathrm{II}} \tag{13}$$

as an additional constraint. This constraint is essentially equivalent to minimizing $(k_s/k_2 - 1)^2$. Hereafter k instead of k_2 will denote the conductivity of sediments.

The two parts, $S^{\rm I}$ and $S^{\rm II}$, are equally weighted here for contributions to the overall S. They can be weighted differently, but the consequence of different weighting is immaterial at the global minimum when $S^{\rm I}$ and $S^{\rm II}$ are both at their minima. It is noted that $(\theta_{\infty s}/\theta_\infty - 1)^2$ can also serve as an alternative to $S^{\rm II}$ or additionally as the third component of the objective function. This constraint is not implemented so that the difference between $\theta_{\infty s}$ and θ_∞ can be used as a criterion to assess the modelling results because the determination of k_s depends on the IM results but $\theta_{\infty s}$ is independently determinable.

Minimization of S with respect to $\mathbf{p}$ (i.e. setting $\partial S/\partial \mathbf{p} = 0$) and solving for the resulted $\mathbf{p}$ iteratively yields at iteration step n,

$$\mathbf{p}_{n+1} = \mathbf{p}^{\rm trial} + \mathbf{C}_{{\rm p}'n}\mathbf{G}_n^{\rm T}\mathbf{C}_{\rm D}^{-1}\left[\left(\mathbf{d}^{\rm obs} - \mathbf{d}_n\right) - \mathbf{G}_n\left(\mathbf{p}^{\rm trial} - \mathbf{p}_n\right)\right] - \mathbf{C}_{{\rm p}'n}\left(f\frac{\partial f}{\partial \mathbf{p}}\right)_n. \quad (14)$$

Except for the final term, which bears the function f, this relation has been derived earlier (Tarantola 1987; Lee 1999, eq. 10.75). The entries of the $N \times M$ sensitivity matrix $\mathbf{G}_n$ are defined by

$$G_{ij} = \left.\frac{\partial d_i}{\partial p_j}\right|_{\mathbf{p}_n}, \quad i = 1, 2, \ldots N; \quad j = 1, 2, \ldots M. \quad (15)$$

This partial derivative is evaluated numerically at the ith computational point (time i) at iteration step n. Matrix $\mathbf{C}_{{\rm p}'n}$ is the post-processing covariance matrix, which is reciprocal to the Hessian,

$$\mathbf{C}_{{\rm p}'n}^{-1} = \mathbf{C}_{\rm p}^{-1} + \mathbf{G}_n^{\rm T}\mathbf{C}_{\rm D}^{-1}\mathbf{G}_n. \quad (16)$$

The term associated with function f in eq. (14) can be derived analytically from the heat release, as computed from the initial temperature rise

$$Q = 2\pi\rho c_1 \int_0^a [\theta_1(r, 0) - \theta_\infty] r\,dr + 2\pi\rho c_2 \int_a^c [\theta_2(r, 0) - \theta_\infty] r\,dr. \quad (17)$$

This Q and ρc_1, ρc_2, θ_1 and θ_2 are understood to be evaluated at iteration step n. The slope η depends on the delay time $t_{\rm D}$ but this dependency becomes insignificant as some of the early-time data are excluded one by one from the linear regression in order to maximize the linear correlation coefficient. Consequently, η is treated as a constant for a given set of cooling data. The derivation for the $M \times 1$ vector $\mathbf{C}_{{\rm p}'n}(f\partial f/\partial \mathbf{p})_n$ is straightforward and the lengthy listing is available from the first author of this paper.

Criteria of model assessment

The results of IM are assessed by three criteria. First, the root-mean-squares (rms) associated with the chosen set of parameters,

$$\text{rms} = \sqrt{\frac{1}{N - M}\sum_{i=1}^{N}\left(d_i^{\rm obs} - d_i\right)^2} \quad (18)$$

should be as small as possible. A suite of rms values can be obtained by running IM with various choices of $\mathbf{p}^{\rm trial}$. However, our test examples indicate that rms alone is not a definitive discriminator because some values of $\mathbf{p}$ may differ from the least to the greatest values by more than 20 per cent, while their rms values are all less than the likely standard error of data. (Here we use the term standard error to mean a measure of the likely error in each individual temperature measurement, not the standard deviation of all the temperature data.) The choice of a final $\mathbf{p}$ becomes murky in such cases.

Hence the distribution of misfits, $\mathbf{d}^{\rm obs} - \mathbf{d}$, is examined as the second criterion, which mandates the misfit distribution for the chosen $\mathbf{p}$ be random around the computed $\mathbf{d}$. Usually good distributions are associated with low rms values. The choices are therefore not sufficiently definitive and need to be narrowed further by imposing the third criterion that the conductivity ratio k_s/k should be as close to one as possible.

A set of $\mathbf{p}$ that meets the conductivity ratio criterion and an rms value of less than the standard error may not always be affiliated with the least rms. In the dilemma of choosing a set of parameters with either the close-to-one ratio or the least rms, we opt for the former because a model with a close-to-one conductivity ratio is almost always associated with an rms that is the least or nearly the least among the models obtained with various $\mathbf{p}^{\rm trial}$. However, the opposite is not necessarily true in the sense that a $\mathbf{p}$ associated with the minimal rms or with an rms less than the standard error of the data may be associated with a ratio that deviates by 20 per cent or more from unity.

A fourth criterion, applicable only for data with long recording duration, is based on extrapolation fitting and will be addressed in the next section. Chi-squared and chi-squared probability were monitored during modelling but the two were not used for model selection because their values are sensitive to the chosen standard data error, which in general is poorly known.

RESULTS AND DISCUSSION

Based on the Newton–Gauss quasi-linear method, the IM algorithm is applicable where $\mathbf{p}^{\rm trial}$ is close to the true but unknown $\mathbf{p}^{\rm true}$. Our Fortran-coded inverse program can crash at run time for a poor assignment of $\mathbf{p}^{\rm trial}$. The selection of $\mathbf{p}^{\rm trial}$ is thus crucial for a successful determination of parameters. To facilitate the choices of $\mathbf{p}^{\rm trial}$, two procedures are adopted. The first procedure is based on a GA that yields a $\mathbf{p}$ (a set of parameters) from likely parameter ranges. The GA output satisfies the survival constraint of near-minimal S through a random combination of parameter retention, exchange, perturbation and recombination as described by Lee *et al.* (2002) for a hydrogeological application except that the random selection of parameters here is based on linear scales instead of logarithmic scales. The GA-produced $\mathbf{p}^{\rm trial}$ typically yields acceptable rms but may also produce a biased misfit distribution or a far-from-one conductivity ratio. The second procedure requires minor adjustments of the GA-produced $\mathbf{p}^{\rm trial}$ prior to inputting it to IM in order to yield a $\mathbf{p}$ that satisfies the model selection criteria. The GA, which expenses more computation time, can be bypassed during the stage of fine-tuning $\mathbf{p}^{\rm trial}$ for IM.

The method is tested with three types of temperature data: three sets of synthetic data, 20 sets of measurements from four heat flow stations in Lake Baikal and seven sets from one station at the Atlantic continental margin off the Carolinas. The Atlantic data set was recorded at intervals of 26 s for approximately 5.5 min, while the data from Lake Baikal were collected at intervals of 2.5 s for 8–11 min. Fine recording intervals avail the details of curve-fitting at early time for a better understanding of the heating and cooling processes. Long recording permits partitioning of a data set for both parameter determination by modelling and parameter validation by extrapolation fitting. Validation by extrapolation serves as

Table 1. Modelling results of synthetic data for station GST3-5.

	ρc_1	$k1$	ρc_2	k_2	θ_0	θ_∞	t_d	w	rms-m	rms-e
True	2.786	0.334	2.959	1.062	3.902	3.601	1.20	0.25		
±0.000	3.175	0.387	3.037	1.097	3.902	3.600	1.03	0.21	0.0015	0.0010
±0.002	3.323	0.373	2.911	1.097	3.905	3.600	1.39	0.16	0.0027	0.0017
±0.005	3.440	0.412	2.824	1.089	3.905	3.600	1.24	0.16	0.0035	0.0032
$\Delta_{0.000}$	14 per cent	16 per cent	2.6 per cent	3.3 per cent	0.000	−0.001	−0.17	−16 per cent		
$\Delta_{0.002}$	19 per cent	12 per cent	−1.7 per cent	3.3 per cent	0.003	−0.001	0.19	36 per cent		
$\Delta_{0.005}$	23 per cent	13 per cent	−4.6 per cent	2.5 per cent	0.003	−0.001	0.04	36 per cent		

Row 'true' represents the parameter values used to generate the synthetic cooling data. See Appendix A for symbols. The '±numbers' are the maxima of random noises (°C) added to the cooling data and the numbers in the cells of these rows are the mean values for four GA-IM runs, with each satisfying $|k_s/k - 1| \leq 0.005$. The values in the cells of the Δ rows denote the model errors in either 100 (mean—true)/true (per cent) or (mean—true) values. θ_0 and θ_∞ are in units of °C and t_d in s.

the fourth criterion for assessing the modelling results of the Lake Baikal data.

Synthetic data

The GA-IM method had been tested with synthetic data before it was applied to the observed data. The results listed in Table 1 are recast for realistic parameter values (the details in modelling are deferred to the next section). Three sets of synthetic data were prepared by adding random noise (with magnitudes up to ±0.000, ±0.002 and ±0.005 K, respectively) to the cooling data synthesized from a set of model parameters for the deepest probe at station GST3 in Lake Baikal. The tabulated values represent arithmetic means for four GA-IM runs. Each run used for the averaging has a conductivity ratio within ±0.005 from the ideal unity value. As indicated in Table 1, the misfit rms increases with increasing levels of random noise in the data. The errors in the determinations of thermal conductivity and heat capacity are within ±5 per cent. The initial and formation temperatures are determined to within 0.002 K of their respective true temperatures for all cases. However, the estimates for the properties of a probe are highly uncertain. The properties and the misfit distributions will be addressed later during the discussion on model uncertainty.

Lake data

25 heat flow stations were successfully completed, using a variant of the violin-bow device (Hyndman *et al.* 1979) in the northern basin of Lake Baikal during a Russian–Belgium expedition during 1997 August. The temperature–conductivity device (Khutortskoy *et al.* 1990; Polyak *et al.* 1996) consists of a 2 m long central support rod and two attached tubes. At 40 mm from the centre rod, the 'temperature tube' (3 mm in outer radius) houses five thermistor sensors spaced at 0.5 m apart vertically. The temperature at the bottom sensor is measured absolutely to an accuracy of 0.005 K while the temperatures at other four sensors are measured relative to the bottom sensor. The temperature resolution is approximately one-half of the accuracy, ∼0.002 K. Each sensor is hereafter referred to as a temperature probe or probe.

Used for *in situ* conductivity measurement, the 'conductivity tube' (2 mm in outer radius) stands diametrically from the temperature tube. It houses four independent 0.5 m long heating wires and four thermistors, each of which is located at the mid-point of its respective heating wire. Each heating wire lies at an equivalent depth between two adjacent thermistors. Conductivity measurements were made for 6 min, starting at 40 s after the penetration of the TC device. The residual effect of frictional heating along the conductivity tube was filtered out with an exponentially decaying time function. Polyak *et al.* (1996) estimated the error of the *in situ* conductivity measurement to be 5 per cent.

The thermal conductivity was measured *in situ* at four of the 25 stations, providing 16 independently measured conductivity values for comparison with the IM-derived values. We used 20 sets of temperature data at those four stations for inverse modelling of the equilibrium temperature and thermal properties. A full report on the heat flow distribution and its tectonic implication will be published elsewhere after the conductivity estimates are completed using the method described herein. Previous studies on heat flow in the lake and in Siberia can be found in Duchkov (1991) and Duchkov *et al.* (1999).

The recording was made at intervals of 2.5 s but only every other data point was included for modelling in order to reduce the computation time. For each probe, 26 data points totalling 130 s in recording duration were modelled. The resulting model parameters were then used to predict the temperatures at every tenth point (or at intervals of 25 s) beyond 130 s. The time step used in the finite-element simulation was 2.5 s for modelling and 6.25 s for extrapolation. The arithmetic mean of nodal temperatures at the centre F_1 and the edge of a probe F_2 is taken as the calculated probe temperature **d**, i.e. $d = (F_1 + F_2)/2$.

Time <40 s

Fig. 1 depicts the first 130 s of the cooling history of five temperature probes at station GST3, which was chosen to show the crossover of the cooling curves for probes 1 and 2. Also shown are the frictional heating events and lake-bottom water temperatures (negative time). According to the heating curves, the penetration took approximately 10–15 s to complete. We assume the heating to have occurred instantaneously but understand that during the course of insertion, frictional heat energy is both being accumulated in the probes and dissipated into the surrounding sediments. In other words, a thin sheath of sediments around each resting probe is pre-heated before the frictional heat energy in the probe begins to dissipate into the formation. The actual heat transfer is further compounded by mass movement (including pore fluid driven to flow by heating-induced fluid pressurization) as a probe squeezes its way into the sediments and by subsequent property changes in the sheath of the disturbed sediments. Generally, a deeper probe is heated to a higher temperature than the shallower one, but as demonstrated by the crossover of cooling curves for probes 1 and 2, the probes can respond distinctly at different sites.

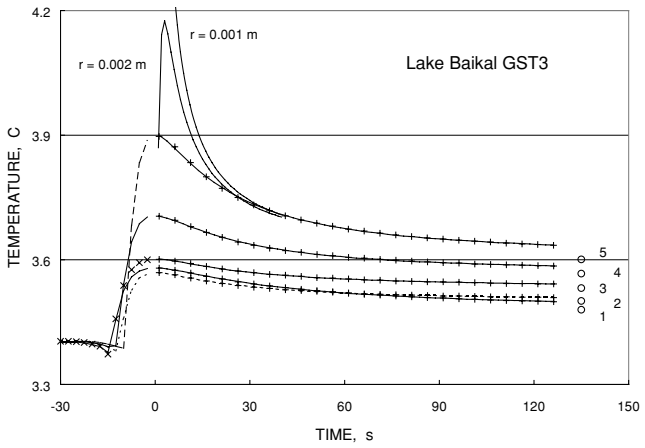

Figure 1. Lake bottom temperature and heating data (time <0) and cooling data and model curves (time >0) at station GST3 in Lake Baikal. Circles denote model equilibrium temperatures. Also depicted are cooling curves at $r = 0.001$ and 0.002 m for an instantaneous line source (located at $r = 0$) that uses parameters derived from probe GST3-5. Note that the temperature at $r = 0.002$ m rises and then cools, signalling the arrival and passing of a heat pulse.

Line sources. Also depicted in Fig. 1 are the cooling curves computed through eq. (11) at $r = 0.001$ and 0.002 m for an instantaneous line source that uses the source parameters and sediment properties derived from probe GST3-5 (Table 1). Note that the time delay in the appearance of peak temperature at $r = 0.002$ m is conspicuous, signalling the approaching and departing heat pulse. For times of less than 40 s, the line-source temperatures are higher than the observed temperatures. This difference suggests that it is inappropriate to model the cooling history as a response to an instantaneous line source.

Beyond 40 s, the two curves merge with the observed and simulated cooling curves at GST3-5. As demonstrated by linear correlation coefficients that exceed 0.99, the asymptotic linearity between the temperature and inverse time also prevails beyond 40 s. The criterion of the conductivity ratio was therefore based on the slope obtained for time periods greater than 40 s. The linear regression was done by removing the early data one by one until the correlation coefficient for the remaining data ($\leq$130 s) exceeds 0.99.

The difference between the line-source curves and the observed cooling curve for times below 40 s at GST3-5 (Fig. 1) reflects the effects of the finite diameter of a probe, the off-axis position of a thermistor and the pre-heating of a sediment sheath around a probe. The energy spreading factor w was introduced by Lee & von Herzen (1994) to account for the pre-heated sheath but its effect was not observable because their recording intervals (26 s) were too coarse to record the imprint in a time of less than 10 s.

Properties of probes. A temperature probe is made of steel casing, thermistor, electric wire and cavity filler. The thermal properties of a probe are difficult to estimate; otherwise the properties of a probe can be fixed to reduce the number of parameters for modelling. The five probes are expected to behave differently. However, the model values for each individual probe also vary from location to location. Overall the heat capacity values range from 2.9 to 4.2 $\times$ 10^6 J m^{-3} K^{-1} and the conductivity values range from 0.22 to 0.50 W m^{-1} K^{-1}. Most of the 20 determinations for the five probes scatter around their respective mean values ($\rho c_1 \approx 3.5 \times 10^6$ J m^{-3} K^{-1} and $k_1 \approx 0.35$ W m^{-1} K^{-1}). Such large uncertainties could be caused by two factors. First, because the thermal properties of an ideal line source are indefinable, the properties of a probe are only estimable with a great uncertainty if most of the data used are of late time when the probe responds as a line source. Secondly, the sediment sheath was disturbed differently to exert a varying influence on the determination. In view of the test results for the synthetic data (Table 1), we conclude that the property of a probe cannot be satisfactorily determined by our method.

Potentially the properties of a probe can be determined with reduced uncertainty if the heating data are also used. Inclusion of the heating data necessitates a thermal model that is more sophisticated than the present one. This idea has not yet been tested. Regardless, the uncertainty in the properties of a probe is not necessarily translated into an equal or greater uncertainty in the estimates of sediment properties, as demonstrated by the results for the synthetic and lake data. As more heat dissipates into a greater sediment volume, the influence of the properties of a probe on the determination of sediment properties diminishes and the accuracy in the determination of thermal properties is attainable to within $\pm$5 per cent.

Model uncertainty

For each probe, four runs of GA were performed within fixed parameter ranges (sediment conductivity from 0.8 to 1.2 W m^{-1} K^{-1} and heat capacity from 2.8 to 3.2 $\times$ 10^6 J m^{-3} K^{-1}). The first recorded and the last modelled cooling data are taken as the lower bounds of initial and equilibrium temperatures, respectively. The delay time lies between 0 and the recording interval (2.5 s) and the energy spreading factor is set between 0 and 1. The outputs from GA are modified iteratively as the input trial parameters $\mathbf{p}^{\text{trial}}$ to IM, for which the parameter ranges are not imposed. The uncertainty in the modelling results are addressed in the categories of conductivity, equilibrium formation temperature, rms and extrapolation misfits.

Conductivity. The results of IM are summarized under the column of $k \pm \sigma$ per cent in Table 2, where k is the arithmetic mean of four conductivity determinations for each set of cooling data and σ is the standard deviation from the mean, expressed as a percentage of the mean. Each individual value chosen for the averaging has a k_s/k ratio that is better than $\pm$0.8 per cent from unity. This σ serves as a measure of internal consistency for those conductivity values that, along with other parameter values, satisfy the model selection criteria. The σ ranges from 2.2 to 12 per cent. A large σ can be reduced by excluding outliers in the k determinations and repeating the GA-IM or by increasing the number of modelling runs. However, the outliers are retained here and the number of runs is capped at four in order to illustrate the reliability or repeatability of the GA-IM if only a single run is conducted.

The k_m column in Table 2 lists the *in situ* measured conductivity values. Each k_m value was measured mid-way between two adjacent temperature sensors where $k \pm \sigma$ per cent are determined; hence strictly speaking, a one-to-one comparison is inappropriate unless the conductivity is homogeneous. Nevertheless, a comparison is made between k_m and the arithmetic mean (column k') of two adjacent model values. The discrepancies Δk ($=k_m - k'$) are less than 0.07 W m^{-1} K^{-1} for 12 of the 16 pairs of comparison. These differences are less than 3.0 per cent from the respective mean values, $(k' + k_m)/2$, and these are within the estimated 5 per cent error for the *in situ* method. A difference of 8–10 per cent appears at the bottom three of the four depth positions at GST2. The cause of such large discrepancies at GST2 is not clear. It is noted that model k at GST2 is associated with low σ. The repeatability of the *in situ*

Table 2. Modelling results for four stations in Lake Baikal.

Probe	$k \pm \sigma$ per cent	k_m	k'	Δk	$\Delta\theta_\infty$	rms-m	rms-e
1-1	0.957 ± 9.6	1.00	1.00	0.00	0.0020	0.0007	0.0017
1-2	1.043 ± 7.1	1.07	1.02	0.05	0.0020	0.0006	0.0017
1-3	0.987 ± 8.6	1.10	1.04	0.06	0.0006	0.0006	0.0004
1-4	1.094 ± 5.6	1.14	1.08	0.06	0.0028	0.0006	0.0006
1-5	1.073 ± 5.3				0.0002	0.0018	0.0010
2-1	0.947 ± 6.2	0.96	1.03	−0.07	0.0003	0.0006	0.0006
2-2	1.110 ± 3.3	0.91	1.11	−0.20	0.0034	0.0009	0.0014
2-3	1.100 ± 3.5	0.96	1.12	−0.16	0.0043	0.0007	0.0018
2-4	1.132 ± 5.5	0.92	1.11	−0.19	0.0019	0.0009	0.0006
2-5	1.093 ± 3.8				0.0039	0.0010	0.0006
3-1	0.904 ± 7.7	0.99	1.06	−0.07	0.0029	0.0006	0.0024
3-2	1.213 ± 4.5	1.04	1.11	−0.07	0.0028	0.0005	0.0023
3-3	$1.000 \pm 12.$	1.01	1.07	−0.06	0.0014	0.0006	0.0026
3-4	1.136 ± 4.0	1.04	1.11	−0.07	0.0020	0.0008	0.0017
3-5	1.085 ± 2.2				0.0005	0.0015	0.0011
4-1	0.777 ± 5.7	0.80	0.82	−0.02	−0.0007	0.0006	0.0035
4-2	0.861 ± 6.9	0.91	0.94	−0.05	−0.0015	0.0006	0.0011
4-3	1.014 ± 4.8	1.04	1.02	0.02	0.0032	0.0006	0.0018
4-4	1.024 ± 7.2	0.96	1.05	−0.09	0.0044	0.0015	0.0033
4-5	1.070 ± 5.3				0.0036	0.0016	0.0039

Symbol $k \pm \sigma$ per cent denotes the mean conductivity of four determinations ($n = 4$) with each satisfying $|k_s/k - 1| \leq 0.008$ and standard deviation $\sigma = \sqrt{\sum_{i=1,n}(k_i - k)^2/(n-1)}$ expressed as a percentage of the mean, k_m is the conductivity measured *in situ* at mid-way between two adjacent temperature sensors, and k' is the corresponding mean of two adjacent values in column $k \pm \sigma$ per cent. $\Delta k = k_m - k'$, $\Delta\theta_\infty = \theta_{\infty s} - \theta_\infty$. Columns $\Delta\theta_\infty$, rms-m, and rms-e represent three of the four criteria used in assessing the modelling results for the curves shown in Fig. 2.

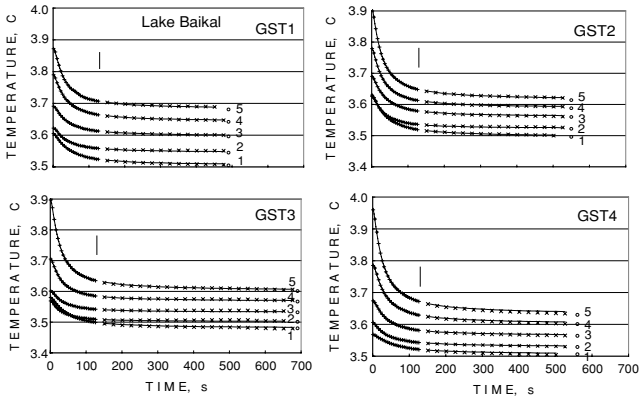

Figure 2. Cooling data and model and extrapolation curves, as demarcated at 130 s by the vertical bar lines, at stations GST1–GST4 in Lake Baikal. Probe positions are spaced at 0.50 m apart vertically. Circles denote model equilibrium temperatures, which are slightly lower than their respective last-recorded temperatures. Note the differences in the cooling responses, especially the crossover between GST3-1 and -2. Some extrapolation curves fit above while others fit below the data systematically even though the misfit rms are less than the measurement errors. (See rms-e in Table 2 and the amplification of misfits in Fig. 3.) A minor perturbation (0.001–0.002 K) to temperature recording appears around 70 s at GST1-5; instability also occurs at GST3-2, -3 and -4 between 350 and 600 s during which the temperature readings creep up, then down relative to the extrapolation curves.

measurements is indeterminable and it is uncertain how effective the residual frictional heat can be removed with an exponential filter for the *in situ* conductivity measurements.

Formation temperature. The model equilibrium temperature θ_∞ is less than their respective last recorded temperatures θ_{last}, stressing the need for a means to obtain the equilibrium temperature even for the unusually long recording time presented here. The asymptotic relation also yields a set of equilibrium temperature $\theta_{\infty s}$, which are higher than θ_∞ in 18 of the 20 case examples (column $\Delta\theta_\infty$). In a few cases, $\theta_{\infty s}$ is higher than θ_{last}. As judged by the cooling trend, the equilibrium temperature should be less than θ_{last} for each depth location. Accordingly, the asymptotic linear regression may not always yield a correct $\theta_{\infty s}$ unless the data beyond 130 s are also included in the regression. In short, through repeated modelling, the equilibrium formation temperatures for the Lake Baikal data are believed to have been well determined to 0.001–0.002 K, which is compatible with the results for the synthetic data.

rms. Fig. 2 depicts the results of curve fitting at the four heat flow stations. Each curve represents a set of model parameters that meets the model selection criteria, as mentioned above. Based on modelling of the first 130 s of the cooling records, the misfits for the individual curves are listed in Table 2 under column rms-m. (The model duration is reported as 2.5 min in the Summary and Conclusion sections for the convenience of expression.) Each set of model parameters is used to predict the cooling behaviour in the period from 130 s to the last recording time ($\leq$11 min). The extrapolation misfits are listed under column rms-e. rms-m and rms-e are less than 0.002 and 0.004 K, respectively (the fourth decimal place listed in Table 2 is insignificant and is shown for resolution comparison only). All rms values, including those used to obtain the mean conductivity but not tabulated here, are less than the estimated accuracy of the temperature measurements (0.005 K). Hence, in terms of the rms criterion alone, all of those sets of model parameters are acceptable and the discrepancies among them represent the uncertainties as measured by σ for an individual GA-IM determination. However, it is worth noting that instability in recording could cause local perturbation in the data trend, as exemplified around 70 s at GST1-5 (Fig. 2), and that the rms for the deepest probe at each station is greater than the shallower ones for all four stations.

The misfit distributions are graphically amplified in Fig. 3 for the best, intermediate and worst fitting in terms of the rms-e tabulated in Table 2. Also depicted are the misfits for the synthetic data. Systematic variations in extrapolation misfits appear in some curves of the former but not the latter.

Extrapolation. Extrapolation fitting cannot be indefinitely extended because the late-time records may be tainted by instrument drift or other uncontrollable physical causes. A combination of plausible causes can produce the systematic misfits: (1) drifting in instrument recording becomes apparent at long recording time. A suspicious symptom of data drift could be seen at GST3-2, -3 and -4 (Fig. 2) where the observed temperatures rise above the simulated cooling curves between 380 and 600 s but retrack those curves henceforth (misfits at GST3-2 are amplified in Fig. 3). (2) A probe could sink slowly in the soft sediments under the weight of the whole TC device; it could also be pulled up slowly if the holding cable of the device is under tension as incurred by a drifting ship; and the entire set of probes could be slowly tilting during long recording. (3) The temperature of a probe could be affected by the frictional heat dissipated from the supporting central rod, which has a greater surface area and hence a greater frictional heating and it lies away at an axis-to-axis distance of 40 mm (less than our FE domain size of 63 mm). The temperature of a probe could creep upward relative to a model curve if scenarios (2) and (3) are significant. (4) Insertion of the central rod drives the pore fluid to flow radially outward while the sediments are being squeezed. This mechanically displaced fluid

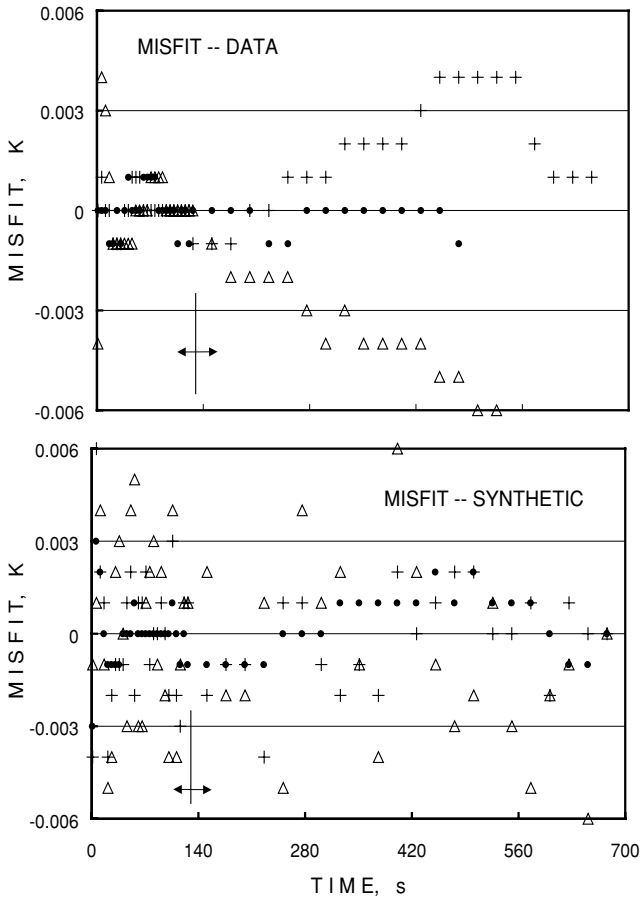

Figure 3. Upper: misfits for the best (•, GST1-3), intermediate (+, GST3-2), and worst (Δ, GST4-5) examples in terms of rms-e (Table 2). Located at 130 s, the vertical bar demarcates modelling and extrapolation misfits. All misfits are plotted after rounding off to the nearest 0.001 K. In the worst case, systematic variations in misfit appear and the first two points have equal misfits but different signs. For the intermediate case, the extrapolation misfits increase with time but decrease toward the end of recording. Lower, misfits for synthetic cooling curves based on parameters for GST3-5: •, noise-free; +, with random noise up to ±0.002 K and Δ, with random noise up to ±0.005 K. Note that misfits increase with the level of data noise but there are no systematic variations.

flow could be enhanced further by fluid pressurization as originated from the differences in thermal expansivity and compressibility between the sediment and the pore fluid (Lee 1996). The front of such a moving fluid may raise the cooling rate of a cooling probe at late times. (5) The model parameters are inaccurately determined. (6) The physical model of cooling of a probe is incorrect, for example, by neglecting the axial (vertical) heat flux.

The misfit distributions for the synthetic data (Table 1, Fig. 3) indicate that the misfits increase with increasing level of data noise but there is no systematic variation in the extrapolation misfits, suggesting that some unknown causes, other than a defective methodology, may affect the late-time field observations. The test on synthetic data cannot assess the significance of axial heat transfer nor the validity of our cooling model but it does extract the conductivity values to within ±5 per cent errors—comparable to the level of uncertainty for the real data.

These six plausible causes of systematic extrapolation misfits cannot be easily assessed or resolved because the rms-e are below the accuracy of temperature measurements and the model rms-m are on a par with the recording resolution. At such low rms values, the set of parameters with the least rms-m or rms-e is not necessarily the best choice. There is no coherent pattern in the distribution of extrapolation misfits (Fig. 2): some curves fit above the data while others fit under it. For a given data set, slight changes in model parameters can revert a fit-above curve to a fit-under curve, or to a perfect matching (e.g. GST1-3 in Fig. 3). The GA in some sense represents a stochastic process and the variations in GA-IM results are indicative of model uncertainty. We prefer the mean values obtained from several GA-IM models, for example, the conductivity values under the column of $k \pm \sigma$ per cent.

The first four of the six plausible causes for systematic extrapolation misfits, if effective, could also affect the *in situ* conductivity measurements. The effect could be too subtle to be perceived and a systematic error in k_m could ensue.

Marine data

Instead of using one long tube that houses five sensors for the lake measurements, the data for our test case of marine heat flow measurements were obtained from seven outrigged probes. The heat flow station was located at the Atlantic continental margin off the Carolinas. The data had been modelled by deleting its first cooling data point and using a built-in empirical relation that links the heat capacity with the thermal conductivity (Lee & von Herzen 1994, station HF2P4). That empirical relation has been abandoned here. Attempts to use all data were successful at five of the seven probes, but failed at probes 4 and 5. As depicted in Fig. 4, the first data point for probe 5 (×) was out of the anticipated cooling trend and therefore was excluded from modelling, although the second point could be the alternative culprit. For probe 4 (Δ), the lack of data to define the course of rapid cooling from the first point to the second would probably have caused numerous run-time crashes if the first point were included. As other interprobe spacings, probes 5 (×) and 6 (+) were spaced 0.6 m apart in depth but the close tracking of their cooling curves are perplexing, possibly as a result of probe displacement.

The time intervals for modelling were fixed at 6.5 s (one quarter of the recording interval). Unlike the lake data recorded at 2.5 s intervals, the history of frictional heating and cooling around

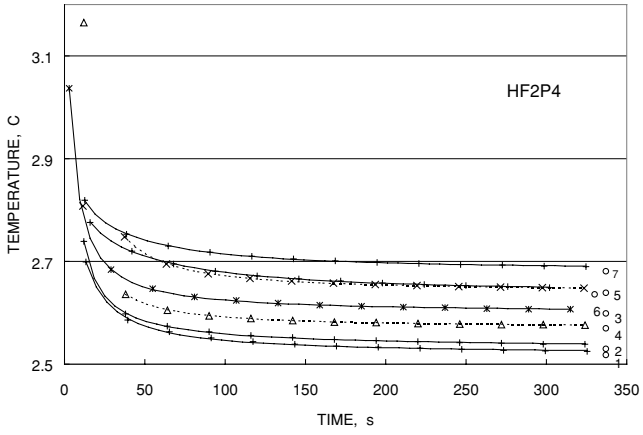

Figure 4. Cooling data and curves for heat flow station HF2P4 at the continental margin off Carolinas (data from Lee & von Herzen 1994). Circles represent equilibrium temperatures with numerals arranged in order of increasing depth, except that probes 3 and 4 are reversed in position. First data points for probes 4 and 5 are excluded from the modelling.

Table 3. Modelling results for station HF2P4 at the Atlantic continental margin off the Carolinas.

Probe	$k \pm \sigma$ per cent	k_m	L&v	Δk	$\Delta\theta_\infty$	rms
1	0.994 ± 4.7	1.048	0.999	0.054	−0.0011	0.0024
2	0.995 ± 4.7	1.069	1.042	0.074	−0.0018	0.0015
3	1.114 ± 7.6	1.114	1.170	0.000	−0.0003	0.0010
4	0.986 ± 6.0	1.002	1.047	0.016	0.0001	0.0007
5	1.106 ± 5.2	1.000	1.079	−0.106	−0.0001	0.0008
6	$0.983 \pm 10.$	1.208	1.140	0.215	−0.0001	0.0011
7	1.129 ± 9.0	1.222	1.202	0.093	0.0002	0.0011

Columns L&v and k_m are from Lee & von Herzen (1994). k_m denotes *in situ* measured conductivity. See Table 2 for other symbols. $\Delta k = k_m - k$.

time zero was poorly observed at Station HF2P4 where the recording interval of 26 s does not provide the required time resolution. As a result, the probe falsely appears to cool in accordance with the expectation of an instantaneous heat release from a line source.

The inclusion of the first data point often led to a run-time crash for deeper penetration probes. The crash can be prevented if the simulated probe temperature is properly represented by the finite-element nodal temperatures at the centre (F_1) and the edge (F_2) of the probe. Weighted more towards the edge temperature for deeper penetration probes, the probe temperature is $(2F_1 + F_2)/3$ for probes 1–4, $(F_1 + F_2)/2$ for probe 5, and F_2 for probes 6 and 7. Table 3 summarizes the modelling results (column $k \pm \sigma$ per cent) for four different runs of GA-IM. All mean conductivities are within one model σ from the k_m as measured with an *in situ* line-source method, except probe 6 where the discrepancy $k_m - k$ is unusually large, 0.215 W m^{-1} K^{-1}. Column L&v represents values from Lee & von Herzen (1994). Column rms represents only the misfits for the cooling curves shown in Fig. 4. All model rms are less than 0.002 K, insignificantly greater than the rms-m for the lake data.

The data trend near the end of recording (Fig. 4) suggests that equilibrium temperatures are attainable only at times much beyond the recording time (∼5 min) at this station unless asymptotic extrapolation or modelling such as that presented here is employed. The two estimates of equilibrium temperature differ by less than ±0.002 K. Since heat flow measurements utilize temperature differences between two adjacent sensors to obtain a geothermal gradient, the absolute values of equilibrium temperatures are inconsequential if the cooling curves (or cooling time constants) are sufficiently similar. However, if temperature data are to be used as records for inferring the history of bottom-water temperature variations or advective fluid seepage, reliable determination of equilibrium temperature is crucial for quality assurance. Fortunately, various sets of $\mathbf{p}^{\text{trial}}$ for each sensor led essentially to the same estimate of equilibrium temperature (<0.002 K) even for those that did not meet the selection criteria.

CONCLUSION

Test results of field data indicate that equilibrium temperature, thermal properties, and hence interval heat flow can be determined from the cooling history of friction-heated probes by means of a finite-element-based, quasi-linear inversion scheme that is also constrained by the asymptotic temperature response to an instantaneous line source. The results of GA need to be refined by an iterative IM because GA misfit distributions are typically biased and the criterion of a close-to-one conductivity ratio is rarely satisfied. As practised here, the GA supplies $\mathbf{p}^{\text{trial}}$ to IM and it is useful for spotting potential local minima of an objective function in the parameter space. The GA results may be acceptable if the ranges of parameters are narrowly defined or the pool of parameter selection is filled with finely discretized parameter values. The restriction on parameter ranges defeats the advantage of using a GA over large ranges of parameter values; and using fine discretization increases the modelling run time. The GA-IM method is a practical combination, with GA scouting the ranges or uncertainty of answers and IM providing model parameters that meet four selection criteria: low rms, unbiased misfit distribution, close-to-one conductivity ratio and low extrapolation misfit.

A 130 s (round up to 2.5 min) long segment of records was bracketed for modelling the data from Lake Baikal but no attempt has been made to determine the shortest duration that is still viable for making an acceptable cooling model. The optimal duration is a function of probe design, frictional heating and sediment properties. We intended to see whether data of short recording duration (approximately half of a typical 5 min duration in marine heat flow measurements) at high recording rates (less than 5 s per reading) are useful. The short duration of recording can save the cost of ship operation time and reduce potential mechanical disturbance arising from keeping the equipmen on the ocean floor for longer. However, recording for over 5 min at high recording rates is still desirable, at some stations interposed among the short-duration stations, for confirmation of the modelling results by extrapolation fitting. Sampling at intervals of 5 s or smaller can facilitate the modelling, especially the cooling behaviour at early times. However, it is cautioned that extrapolation fitting should not be carried too far beyond the range of time used in the GA-IM modelling because several plausible causes (e.g. recording drift, incidental probe movement, heat dissipated and fluid driven from a centrally located supporting rod or core bearer) can subtly influence the late-time data.

Our tests indicated that the equilibrium temperature can be determined within ±0.002 K from 130 s of recording, even for some models that do not satisfy the criteria of a close-to-one conductivity ratio and an rms on par with the standard error of data. The uncertainty in the determination of conductivity and diffusivity (heat capacity is used in modelling) is probably around 5 per cent but it can reach 10 per cent for one individual set of model parameters, as assessed by comparing the model conductivity with the independently measured conductivity and by making multimodel runs of GA-IM. The high uncertainty can be reduced by excluding outliers or, as done here, by using the mean values of the results from multimodelling runs.

ACKNOWLEDGMENTS

We appreciate the insightful comments by Dr Kelin Wang, Dr Paul Shen and an anonymous reviewer.

REFERENCES

Barker, P.F. & Lawver, L.A., 2000. Anomalous temperatures in central Scotia Sea sediments—bottom water variation or pore water circulation in old oceanic crust, *Geophys. Res. Lett.,* **27,** 13–16.

Bullard, E.C., 1954. The flow of heat through the floor of the Atlantic Ocean, *Proc. R. Soc. Lond.,* A., **222,** 408–429.

Davis, E.E. *et al.*, 1999. Regional heat-flow variations across the sedimented Juan de Fuca Ridge eastern flank: constraints on lithospheric cooling and lateral hydrothermal heat transport, *J. geophys. Res.,* **104,** 17 675–17 688.

Davis, E.E., Wang, K. & Becker, K., 2002. Comment on Geli *et al.*, 2001. *EOS, Trans.,* **83,** 196–197.

Duchkov, A.D., 1991. Review of Siberian heat flow data, in *Terrestrial Heat Flow and Lithosphere Structure,* pp. 426–443, eds Chermak, V. & Rybach, L., Springer-Verlag, Berlin.

Duchkov, A.D., Lysak, S.V., Golubev, V.A., Dorofeeva, R.P. & Sokolova, L.S., 1999. Heat flow and geothermal field of the Baikal region, *Russian Geol. Geophys.,* **40,** 289–304.

Fisher, A.T. *et al.*, 2002. Comment on Geli *et al.* (2001). *EOS, Trans.,* **83,** 196–196.

Geli, L. *et al.*, 2001. Deep-penetration heat flow probes raise questions about interpretations from shorter probes, *EOS, Trans. Am. geophys. Un.,* **82,** 317.

Hutchison, I. & Owen, T., 1989. A microprocessor heat flow probe, in *Handbook of Seafloor Heat flow,* pp. 91–120, eds Wright, J.A. & Louden, K.E., CRC Press, Boca Raton, FL.

Hyndman, R.D., Davis, E.E. & Wright, J.A., 1979. The measurement of marine geothermal heat flow by a multi-penetration probe with digital acoustic telemetry and *in situ* thermal conductivity, *Mar. Geolphys. Res.,* **4,** 181–205.

Jemsek, J. & von Herzen, R.P., 1989. Measurement of in situ sediment thermal conductivity: continuous-heating method with outrigged probe, in *Handbook of Seafloor Heat Flow,* pp. 91–120, eds Wright, J.A. & Louden, K.E., CRC Press, Boca Raton, FL.

Khutortskoy, M.D., Fernandez, R., Kononov, V.I., Polyak, B.G., Matveev, V.G. & Rot, A.A., 1990. Heat flow through the sea bottom around Yucatan Peninsula, *J. geophys. Res.,* **95,** 1223–1237.

Lee, T.-C., 1996. Pore pressure rise, frictional strength, and fault slip: one-dimensional interaction models, *Geophys. J. Int.* **125,** 371–384.

Lee, T.-C., 1999. *Applied Mathematics in Hydrogeology,* p. 382, Lewis Publishers, New York.

Lee, T.-C. & von Herzen, R.P., 1994. *In-situ* determination of thermal properties in sediments using friction-generated probe source, *J. geophys. Res.,* **99,** 12 121–12 132.

Lee, T.-C., Perina, T. & Lee, C.-Y., 2002. Validation of aquifer parameter determination by extrapolation fitting and treating thickness as an unknown, *J. Hydrology,* **265,** 15–33.

Lister, C.R.B., 1979. The pulse probe method of conductivity measurement, *Geophys. J. R. astr. Soc.,* **57,** 451–461.

Polyak, B.G. *et al.*, 1996. Heat flow in the Alboran Sea, the western Mediterranean, *Tectonophysics,* **263,** 191–218.

Tarantola, A., 1987. *Inverse Problem Theory,* p. 613, Elsevier, New York.

von Herzen, R.P., Ruppel, C., Molnar, P., Nettles, M., Nagihara, S. & Ekstrom, G., 2001. A constraint on shear stress at the Pacific–Australian plate boundary from heat flow and seismicity at the Kermadec Forearc, *J. geophys. Res.,* **106,** 6817–6833.

APPENDIX A: NOTATION AND ABBREVIATIONS

Symbol	Definition	Symbol	Definition
a	Radius of a sensor probe (m)	b	Outer radius of a sediment sheath (m)
c	$\approx$ infinite distance (m)	$\mathbf{C}$	Capacitance matrix (J m^{-1} K^{-1})
$\mathbf{C}_\mathrm{d}$	Covariance matrix, data (K^2)	$\mathbf{C}_\mathrm{p}$	Covariance matrix, parameter
$\mathbf{C}_{\mathrm{p}'}$	$\mathbf{C}_\mathrm{p}$, post-processing	$\mathbf{d}$	Temperature vector, computed (K)
D	Diffusion distance (m)	$\mathbf{d}^\mathrm{obs}$	Temperature vector, observed (K)
f	$=k_\mathrm{s}/k-1$	FE	Finite element
F_1	Temperature at $r=0$ (K)	F_2	Temperature at $r=a$ (K)
$\mathbf{G}$	Sensitivity matrix, $\partial\mathbf{d}/\partial\mathbf{p}$	GA	Genetic algorithm
IM	Inverse modelling	k	Conductivity (W m^{-1} K^{-1})
$\mathbf{K}$	Conductance matrix (W m^{-1} K^{-1})	k_s	k, asymptotic relation
k_1	k, probe	k_2	k, sediment
M	Number of parameters	N	Number of data points
N_r	Number of ring elements	$\mathbf{p}$	Parameter vector
$\mathbf{p}^\mathrm{trial}$	Trial parameter vector	Q	Heat generation/length (J m^{-1})
r	Radial distance (m)	$\bar{r}$	Mean nodal distance (m)
rms	Root mean square (K)	rms-m	rms, model
rms-e	rms, extrapolation	S	Objective function
S^I	Objective function, I	S^II	Objective function, II
t	Time (s)	t_D	Delay time (s)
TC	Temperature–conductivity	w	Energy spreading factor
$\boldsymbol{\theta}$	Temperature (K)	θ	Temperature vector, nodal (K)
$\boldsymbol{\theta}_b$	Temperature at $r=b$ (K)	θ_0	Initial temperature (K)
$\boldsymbol{\theta}_1$	Temperature, probe (K)	θ_2	Temperature, sediment (K)
$\boldsymbol{\theta}_\infty$	Equilibrium temperature (K)	$\theta_{\infty\mathrm{s}}$	θ_∞, asymptotic relation
η	$=Q/4\pi\ k_\mathrm{s}$ (K s)	κ	Thermal diffusivity (m^2 s^{-1})
ρc	Heat capacity (J m^{-3} K)	$(\rho c)_1$	ρc, probe
$(\rho c)_2$	ρc, sediment	Δr	Element thickness (m)
Δt	Time step (s)		

Note: each entry of matrices $\mathbf{C}_\mathrm{p}$, $\mathbf{C}_{\mathrm{p}'}\mathbf{G}$ and $\mathbf{p}^\mathrm{trial}$ depends on the physical units of parameters $\mathbf{p}$.